Hentschke *Nanoscale Research Letters* (2016) 11:88
DOI 10.1186/s11671-015-1188-5

Nanoscale Research Letters
a SpringerOpen Journal

NANO EXPRESS Open Access

On the specific heat capacity enhancement in nanofluids

Reinhard Hentschke

Abstract

Molten salts are used as heat transfer fluids and for short-term heat energy storage in solar power plants. Experiments show that the specific heat capacity of the base salt may be significantly enhanced by adding small amounts of certain nanoparticles. This effect, which is technically interesting and economically important, is not yet understood. This paper presents a critical discussion of the existing attendant experimental literature and the phenomenological models put forward thus far. A common assumption, the existence of nanolayers surrounding the nanoparticles, which are thought to be the source of, in some cases, the large increase of a nanofluid's specific heat capacity is criticized and a different model is proposed. The model assumes that the influence of the nanoparticles in the surrounding liquid is of long range. The attendant long-range interfacial layers may interact with each other upon increase of nanoparticle concentration. This can explain the specific heat maximum observed by different groups, for which no other theoretical explanation appears to exist.

Keywords: Energy storage, Solar power plants, Heat transfer nanofluids, Specific heat capacity

Background

A standard problem in courses on Statistical Mechanics, when the topic is Stefan's law, is the calculation of the size of a "solar panel" large enough to collect the energy currently consumed by the earth's population. Even though this is an academic problem, the resulting area is surprisingly small, providing a feeling for the vast amount of solar energy received by the surface of the earth. One of the technologies, being developed in this context, is that of thermal solar power plants, especially of the parabolic trough and power tower types. Inside these plants, heat transfer fluids, e.g., molten salts, are used for energy transport as well as storage [1]. Heat transfer fluids must meet certain key criteria - aside from being inexpensive. They should be thermally stable at high temperatures. Their melting point should be as low as possible. The same is true for their vapor pressure at high temperatures (several hundred degree Celsius). Other aspects include corrosivity, viscosity, thermal conductivity, toxicity, etc.

The thermodynamic property of interest in this study is the specific heat capacity, i.e., the heat capacity in units of joules per gram Kelvin, of the heat transfer fluid, which should be as high as possible. The aforementioned molten salts or rather salt mixtures do possess a wide temperature range of useful application - an advantage outweighing their comparatively low specific heat capacity of about 0.75 to 2 J/(gK). However, a number of experiments (cf. the recent review [2]) do show that the specific heat capacity of the base salt mixture, here and in the following we talk about c_P, the specific heat capacity at constant pressure, is substantially enhanced by addition of nanoparticles in small amounts (≈ 1 wt.%), i.e., particles whose size distribution is peaked around 10 to 100 nm. Salt mixtures doped with nanoparticles belong to a larger and more general class of fluids, so-called nanofluids.

Nanofluids doped with suspended nanoparticles do show enhanced thermal conductivities [3–8]. The effect of nanoparticle addition on the specific heat capacity of the fluids, however, does not yield a consistent picture (e.g., [9–37]). Das and co-workers [9–11] find reduced specific heat capacities of nanofluids consisting of silicon dioxide, zinc oxide, and alumina nanoparticles, respectively, dispersed in a mixture of water and ethylene glycol compared to the base fluid. The specific heat capacity of the nanofluid is found to decrease with increasing nanoparticle concentration. Zhou and Ni [12] also find a reduced specific heat capacity of the water-based alumina

Correspondence: hentschk@uni-wuppertal.de
Fachbereich Mathematik und Naturwissenschaften, Bergische Universität, D-42097 Wuppertal, Germany

nanofluid and a similar decrease of specific heat capacity with increasing particle concentration. An extensive study by O'Hanley et al. [13] confirms this detrimental effect of various types of nanoparticles on the heat capacity of water. Recent work by Sekhar and Sharma [14] comes to similar conclusions. In contrast, Nelson et al. [15] find that c_P of polyalphaolefin is enhanced by 50 % when mixed with graphite nanoparticles at 0.6 % mass fraction. The c_P of Li_2CO_3/K_2CO_3 eutectic salt is enhanced by 19 % when mixed with carbon nanotubes at 1 % mass fraction as reported by Shin et al. [16]. Refs. [17, 18] by Jo and Banerjee are continuations of this work using the same base fluid. In [17], the effect of nanoparticle dispersion is studied based on graphite nanoparticles. Greater enhancement in the specific heat capacity was observed from the nanomaterial samples with more homogeneous dispersion of the nanoparticles. In [18], multiwalled CNTs (carbon nanotubes) were dispersed using a surfactant (SDS) to obtain homogeneous dispersion. Four different concentrations (0.1, 0.5, 1, and 5 wt.%) of CNT were employed. It was observed that the specific heat capacity is enhanced by doping with the nanotubes in both solid and liquid phase. In addition, the enhancements of the specific heat capacity are increased with increase of the CNT concentration. Zhou et al. [19] find a maximum enhancement of about 6 % of the specific heat capacity of their ethylene glycol-based CuO nanofluid. In addition, Shin and Banerjee [20–22] obtain specific heat capacity enhancements of about 14 and 19 % to 24 % in different nanofluids, i.e., Li_2CO_3/K_2CO_3 eutectic and chloride eutectic, doped with 1 wt.% SiO_2 nanoparticles. Most recently, they report specific heat capacities in the Li_2CO_3/K_2CO_3 (62:38) eutectic doped with 1.5 wt.% silica nanoparticles (size between 2 and 20 nm), which are about 120 % above the base salt specific heat capacity [23]. These researchers have also used alumina nanoparticles in again the same base salt mixture [24]. They report an enhancement of around 30 % at 1 % mass concentration. Lu and Huang [25] study the $NaNO_3/KNO_3$ (60:40) liquid base salt mixture doped with alumina nanoparticles of two distinct sizes. Their key observation is that c_P is larger for the nanofluid containing the larger nanoparticles under otherwise identical conditions. This is also found by Dudda and Shin [26] in $NaNO_3/KNO_3$ (60:40) doped (1 wt.%) with SiO_2 nanoparticles. In contrast, Tiznobaik and Shin [27] do find no influence of particle size in the Li_2CO_3/K_2CO_3 eutectic doped with silicon dioxide nanoparticles (5, 10, 30, and 60 nm in diameter - same sizes as in [26]). In another publication, Tiznobaik and Shin [28] tie the enhancement of the specific heat capacity observed in the previous system to the formation of nanostructures surrounding the particles. In subsequent work Shin, Tiznobaik, and Banerjee [29] discuss the possible role of fractal flocs formed by the nanoparticles on the enhancement of the specific heat capacity in nanofluid. The two investigations by Chieruzzi [30] and Lasfargues et al. [31, 32] study the eutectic mixture of $NaNO_3/KNO_3$ doped with different nanoparticles at different concentrations. These researchers find that in general the specific heat capacity is enhanced by a few percent (up to about 10 % using copper oxide in [31]). Most notably, however, a maximum enhancement is observed in the range between 0.1 and 1 wt.% nanoparticle. An analogous maximum was also observed by Heilmann [33] using the same base salt doped with Al_2O_3 nanoparticles. Another confirmation of the maximum comes from Andreu-Cabedo [34]. They study the eutectic mixture of $NaNO_3/KNO_3$ doped with silica nanoparticles in the concentration range from 0.5 to 2 wt.%. Their maximum heat capacity increase is 25 %.

It is important to stress that the observation of enhanced heat capacity is not limited to nanofluids whose base is a binary mixture. Recently, Chieruzzi et al. [35] have studied a single component base fluid, KNO_3, doped with different size nanoparticles of silica, alumina, and a mix thereof. In both the solid and the liquid phase, the authors do observe an increase of c_P. At 1 wt.% added nanoparticles c_P in the solid phase is increased between 5 and 10 %. In the liquid phase, the increase is around 6 %. Ho and Pan [36] have looked for the optimal concentration of alumina nanoparticles in a molten ternary salt mixture. They obtain a specific heat capacity increase of about 20 % at a very small nanoparticle concentration, i.e., 0.063 wt.%. A still larger increase of c_P has been found by Paul [37], who has studied different nanoparticle-enhanced ionic liquids. Ionic liquids are salts whose cations are large organic species and anions are organic or inorganic species. Interestingly, the considerable increases of c_P reported in this work appear to be monotonous functions of nanoparticle volume fraction in the entire range of volume fractions studied (up to 2.5 wt.%).

In summary, it is probably safe to say that the specific heat capacity of salt mixtures is enhanced by every type of nanoparticle used. The particle mass concentration should not exceed 1 wt.%, however. Details of the methods of preparation may vary (e.g., the temperatures during drying of the samples). Quite independent of these variations, c_P enhancements are between 10 and 30 % on average. Doping water with nanoparticles thus far yields a decrease of the heat capacity. A molecular theory explaining the above effects of nanoparticles on the specific heat capacity of heat transfer fluids does not yet exist.

Results and Discussion

The first part of this section, phenomenological heat capacity of nanofluids - the nanolayer concept, is an exposition of the existing phenomenological theory and where it fails to describe the experimental findings. The second part, phenomenological heat capacity of nanofluids - the

mesolayer concept, presents arguments in support of the idea that the effect of the nanoparticles on the base fluid should be of much longer range than assumed previously. In the third part, the interacting mesolayer model, it is shown how this concept can be developed into a model explaining the specific heat maximum observed in several experimental studies. The section concludes with a suggestion on how to tie this phenomenological theory to molecular interaction.

Phenomenological heat capacity of nanofluids - the nanolayer concept: In certain simple cases, the dependence of the specific heat capacity of the nanofluid is well described by

$$c_P = \frac{M_{\rm liq} c_{P,\rm liq} + M_{\rm np} c_{P,\rm np}}{M_{\rm liq} + M_{\rm np}}. \quad (1)$$

Here $M_{\rm liq}$ is the mass of the base liquid, whereas $M_{\rm np}$ is the total mass of the nanoparticles. $c_{P,\rm liq}$ and $c_{P,\rm np}$ are the respective specific heat capacities of the two components. More precisely speaking, there are more than two components present if the base liquid is a mixture. The dashed lines in the top panel of Fig. 1 show this equation in comparison to experimental data from [13]. Notice that the volume fraction in the figure refers to volume fraction nanoparticles, ϕ, related to the mass ratio $y = M_{\rm np}/M_{\rm liq}$ via

$$\phi = \frac{y/\rho_{\rm np}}{y/\rho_{\rm np} + 1/\rho_{\rm liq}} \quad \text{or} \quad y = \frac{\rho_{\rm np}}{\rho_{\rm liq}} \frac{\phi}{1-\phi}, \quad (2)$$

where $\rho_{\rm liq}$ and $\rho_{\rm np}$ are the mass densities of the base liquid and the nanoparticles, respectively. In [13], the authors investigate water-based silica, alumina, and copper oxide nanofluids. In some cases, Eq. 1, e.g., the open symbols in the top panel of Fig. 1, provides a good description of the experimental data. In other cases, e.g., the closed symbols in the top panel of Fig. 1, Eq. 1 is off.

It is worth noting that the specific heat capacity of the nanoparticles, $c_{P,\rm np}$, is significantly below the specific heat capacity of the base fluid, $c_{P,\rm liq}$ - and not only in the case of water. Theoretical calculations of $c_{P,\rm np}$ indicate that the nanoparticles possess somewhat larger specific heat capacities (at high temperatures) than their bulk materials [38, 39]. However, the difference does not alter this statement. In particular, the concentration of nanoparticles in the experiments is so small that the difference between the nanoparticle's $c_{P,\rm np}$ and the corresponding bulk-specific heat capacities is negligible in the present context.

Equation 1 may be improved by addition of an interface or nanolayer separating the bulk base fluid from the nanoparticle's surface as has been done in [25] (Eq. 2) (cf. also [26] (Eq. 2)). It is assumed that this interface possess a characteristic thickness of between a couple to

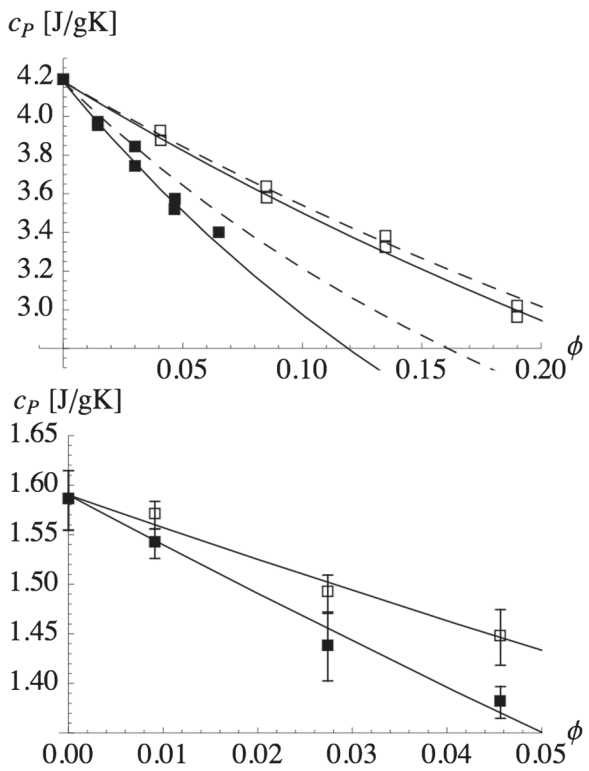

Fig. 1 Specific heat capacity of the nanofluid vs. particle volume fraction. *Top*: Specific heat capacity of water-based nanofluids. Experimental data are taken from Figs. 2 and 8 in [13] (*open symbols*: silica; *closed symbols*: alumina). The temperature is 45 °C. *Dashed lines*: Eq. 1. *Solid lines*: Eq. 5 using $\lambda = 1.05$ (silica) and $\lambda = 1.2$ (alumina). *Bottom*: Specific heat capacities for $NaNO_3/KNO_3$ (60:40) doped with alumina nanoparticles. *Symbols*: data from Figure 5 in [25]. Two different size nanoparticles are used: 13 nm (*solid symbols*) and 90 nm (*hollow symbols*). *Solid lines*: Eq. 5 using $\lambda = 2.2$ (13 nm particle size) and $\lambda = 1.7$ (90 nm particle size). The other quantities needed to evaluate Eq. 5 were taken from [25]

10 nm. This interface contribution is introduced into the numerator of Eq. 1, i.e.

$$c_P = \frac{(M_{\rm liq} - M_i) c_{P,\rm liq} + M_i c_{P,i} + M_{\rm np} c_{P,\rm np}}{M_{\rm liq} + M_{\rm np}}. \quad (3)$$

Here, M_i is the mass of the base liquid in the interface around the nanoparticles, and $c_{P,i}$ is the specific heat capacity associated with the interface. In addition, we define

$$\kappa = \frac{c_{P,i}}{c_{P,\rm liq}}. \quad (4)$$

κ is a factor by which the specific heat capacity in the interface differs on average from the specific heat capacity in the pure bulk fluid. Thus, Eq. 3 becomes

$$c_P = c_{P,\rm liq} + x_{\rm np} \left(c_{P,\rm np} - \lambda c_{P,\rm liq} \right), \quad (5)$$

with

$$\lambda = 1 + (1-\kappa)\frac{M_i}{M_{\rm np}} \ . \tag{6}$$

The quantity $x_{\rm np} = 1 - x_{\rm liq} = M_{\rm np}/(M_{\rm np} + M_{\rm liq})$ is the mass fraction nanoparticles (notice: $x_{\rm np} = y/(1+y)$). In the limit $\lambda = 1$ (or $\kappa = 1$), this equation is identical to Eq. 1. However, if momentarily we treat λ as an adjustable parameter, we can improve the approximation to the data in Fig. 1 (solid lines in the top panel), which suggests that the concept of an interfacial layer indeed possesses significance.

The bottom panel of Fig. 1 shows experimental results obtained by Lu and Huang [25]. These researchers study the $NaNO_3/KNO_3$ (60:40) liquid base salt mixture doped with alumina nanoparticles of two distinct sizes. Their key observation is that c_P is larger for the nanofluid containing the larger nanoparticles under otherwise identical conditions. Using again Eq. 5, we find reasonable agreement with the experimental data when λ is around 2.

But how is λ related to the interface? A standard technical specification available for nanoparticles is their surface area per mass unit, A (usually given in m^2/g). This surface is determined using different probe molecules, i.e., small ones like nitrogen or larger ones like CTAB. Typical values are on the order of 100 m^2/g. Actual values may deviate from this one by factors between 2 and 3. However, for the present discussion, this is not essential. Specifically, we can estimate the mass ratio $M_i/M_{\rm np}$ via $M_i/M_{\rm np} \approx A\rho_{{\rm liq},i}\Delta$. Here $\rho_{{\rm liq},i}$ is the average liquid density in the interfacial layer with thickness Δ. Furthermore, it is interesting to note that A is found to be inversely proportional to the particle radius R (cf. [40]) as shown in Fig. 2. Using this estimate $M_i/M_{\rm np}$, Eq. 6 becomes

$$\lambda - 1 \approx (1-\kappa)A\rho_{{\rm liq},i}\Delta \ . \tag{7}$$

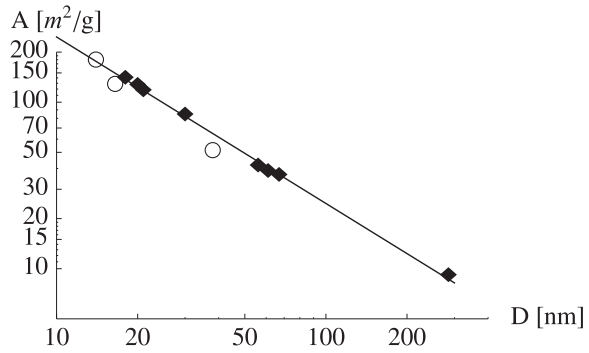

Fig. 2 Specific surface area, *A*, vs. particle diameter, *D*. *Diamonds*: N_2-BET data for carbon black from [40] (table 3.10 (p. 282); *circles*: N_2-BET data for silica from [40] (table 3.19 (p. 300). The solid line is a $A \propto D^{-1}$-fit to the carbon black data

What does this mean for the λ values used in the bottom panel of Fig. 1? Suppose we use $A \approx 150$ m^2/g for the small particles and $A \approx 30$ m^2/g for the large particles. In addition, we set $\rho_{{\rm liq},i} \approx \rho_{\rm liq} \approx 1.8$ g/cm^3 (cf. [25]). Of course, the particles induce structuring of the liquid close to their surface [41] and thus this may or may not be a good approximation. But it is fully sufficient if we want to explore the basic consequences of the interface. If we assume $\Delta = 10$ nm, then we need $\kappa \approx 0.55$ for the small particles and $\kappa \approx -0.30$ for the large ones. Negative values for κ are in violation of thermal stability, however. We can avoid this by increasing the other quantities, i.e., A, $\rho_{\rm liq}$ or Δ. For instance, assuming $\Delta = 100$ nm, we obtain $\kappa \approx 0.96$ in case of the small particles and $\kappa \approx 0.87$ in the case of the large particles. Now the κ values are reasonable, but the width of the interface is unexpectedly large.

Phenomenological heat capacity of nanofluids - the mesolayer concept: The above discussion suggests that the nanoparticles induce a far reaching effect in the surrounding liquid. Of course, there is also the possibility that κ instead of Δ may become large, i.e. $c_{P,i} \gg c_{P,{\rm liq}}$. Even though large or diverging specific heat capacities may occur at a phase transition, i.e., in particular a second-order transition, these conditions are rather special and strongly temperature dependent [42]. Therefore, it is worth noting that most authors do observe only a slight change, usually a slight linear increase, of c_P in a fairly large temperature interval in the liquid state of the nanofluid (examples include Figs. 2 and 3 in [21], Fig. 3 in [23], Fig. 2 in [26], Figs. 2, 3, and 4 in [27], or Fig. 1 in [34]). All in all, a mechanism which increases $c_{P,i}$ by a factor greater than two compared to the base fluid and at the same time is weakly dependent on temperature is difficult to imagine.

Next, we focus on recent work by Shin and Banerjee [23]. These authors find increases of the specific heat capacity of over 120 % relative to the base fluid (Li_2CO_3/K_2CO_3) (62:38). The nanoparticles are silica particles. The authors assume a κ of around 4. However, they do not provide a mechanism explaining this large increase of $c_{P,i}$ relative to $c_{P,liq}$. They also try to avoid large interface widths by proposing that the main effect is due to small nanoparticles with diameters of around 2 nm. This however makes it difficult to fix the attendant mass fraction (the overall $x_{\rm np}$ is around 1.5 wt.%). Small particles, as is illustrated in Fig. 2, do possess a large surface area. Thus, one may obtain a sufficiently large value for λ, according to Eq. 7, with a moderate Δ.

There is another subtlety worth mentioning. Apparently, the authors do observe segregation of their nanofluid into two "phases," called types A and B, during preparation. The large increases of c_P reported in the paper are solely observed in the type A nanofluid,

apparently containing well-dispersed nanoparticles <20 nm. However, it is not clear how large the mass content nanoparticle really is in type A. If we calculate the average center of mass separation for 2-nm particles at 1.5 wt.%, we obtain around 7 nm (on a cubic lattice). However, the transmission electron micrograph of a type A sample printed in the paper shows particles separated much farther than this. The picture is consistent with 20-nm particles as the dominant species, which yield an average separation of around 70 nm. For these particles, we obtain $\Delta \approx 50$ nm if $\kappa = 4$ is assumed. Because large κ values, and 4 already is large, are difficult to rationalize, this again suggest that Δ is in the 100-nm range. It is also worth mentioning that in a previous publication, the same authors [22], based on the same system (with a different silica supplier), do find a mere 20 % enhancement of c_P. The reason for this substantial discrepancy is not clear.

Finally, we want to address the experimental observation of a maximum specific heat as a function of nanoparticle concentration. In Eq. 5, c_P depends linearly on $x_{\rm np}$. Therefore, this "theory" cannot describe results where c_P plotted vs. nanoparticle concentration is not monotonous. Figure 3 (top panel) shows measurements of Heilmann [33], which exhibit a rather distinct maximum at 1 wt.%. Unfortunately, if we include data by two other groups, i.e., Chieruzzi et al. [30] and Lasfargues et al. [32], matters become less clear as shown in Fig. 3. Open squares connected via a solid line are data obtained by Chieruzzi et al. [30] for the same system. We notice that while Chieruzzi et al. also obtain a maximum at 1 wt.%, their c_p of the plain salt mixture is significantly higher than Heilmann's at roughly the same temperature. Thus, Chieruzzi et al. observe an initial decrease of c_P. This is also true if they use TiO_2 (open circles) or SiO_2 (open down triangles) nanoparticles. Their maximum at 1 wt.% in the case of SiO_2 is in rough accord with the data obtained by Andreu-Cabedo et al. [34] for the same system (solid down triangles). In the case of TiO_2, Chieruzzi et al.'s results can be compared to the results obtained by Lasfargues et al. [32]. Aside from the discrepancy of the c_P values of the base salt, Lasfargues et al. find their c_P maximum at significantly lower concentration. The large scatter exhibited by c_P obtained for the pure base salt in the different studies (at about the same temperatures) illustrates that differences in the system preparation or (slight) differences in composition tend to obscure the overall picture.

The interacting mesolayer model: There is an explanation for the observed c_P maximum if we accept the above idea that the "interfacial layer" induced by a nanoparticle in the surrounding fluid is significantly wider than currently assumed. Notice that Eq. 5 does not account for the overlap between "interfacial layers" of nanoparticles. There is of course no need for this within the nanolayer concept, because at the nanoparticle concentrations of interest , no significant overlap of nanolayers occurs. If the layers are much wider, then overlap occurs even at very small nanoparticle concentrations, and this, as we shall see, can produce the c_P vs. $x_{\rm np}$ maximum.

We can extend Eq. 5 to include this idea as follows. The total mass of the entire system, M, is, as already pointed out, composed of three distinct contributions, i.e.,

$$M = M_{{\rm liq},b} + M_i + M_{\rm np} \; . \tag{8}$$

Here, $M_{{\rm liq},b}$ is the mass of the bulk liquid not affected by the presence of nanoparticles. M_i is the mass of the liquid affected by the nanoparticles, i.e., the mass of all interface layers combined. $M_{\rm np}$ is the mass of all nanoparticles combined. If we keep on adding nanoparticles, then we may reach a concentration when

$$M_{{\rm liq},b} = 0 \; . \tag{9}$$

There simply is no bulk liquid left unaffected by the presence of nanoparticles. Beyond this concentration, Eq. 5 is no longer valid. It is replaced by the equation

$$c_p = \frac{M_i c_{P,i} + M_{\rm np} c_{P,{\rm np}}}{M} \tag{10}$$

or

$$c_p = \kappa c_{P,{\rm liq}} + x_{\rm np} \left(c_{P,{\rm np}} - \kappa c_{P,{\rm liq}} \right) \tag{11}$$

using the above terminology. The crossover mass fraction, $x'_{\rm np}$, beyond which Eq. 5 should be replaced by Eq. 11 according to Eq. 9 is

$$x'_{\rm np} = \frac{1}{1 + M_i/M_{\rm np}} \; . \tag{12}$$

In reality, there is no distinct $x'_{\rm np}$, because the interfacial shells influenced by the individual nanoparticles will begin to overlap gradually upon increasing the nanoparticle concentration. Nevertheless, we are interested in the basic consequences of the overlap for which this crude model is sufficient. Figure 4 shows the result of this new model, i.e., Eq. 5 in conjunction with Eqs. 11 and 12, (solid line) in comparison to the data of Lasfargues et al. [32] from Fig. 3 (bottom panel). We use the experimental values for $c_{P,{\rm liq}}$ and $c_{p,{\rm np}}$. κ and $M_i/M_{\rm np}$ are adjustable parameters. Here, $\kappa = 1.035$ and $M_i/M_{\rm np} = 200$. The required increase of $c_{P,i}$ in comparison to $c_{P,{\rm liq}}$ is quite small (about 4 %). The width of the interfacial layer, Δ, however is about 4 times the diameter of the nanoparticles. We have assumed that the density of the bulk liquid is the same as the density of the liquid in the interface layer. Even though computer simulations have shown that solid surfaces may induce pronounced density variations in a liquid, the latter rarely extend beyond three to four molecular diameters away from the surface (e.g., [43]). Thus, the average density in the wide layer considered here remains close to the liquid bulk density.

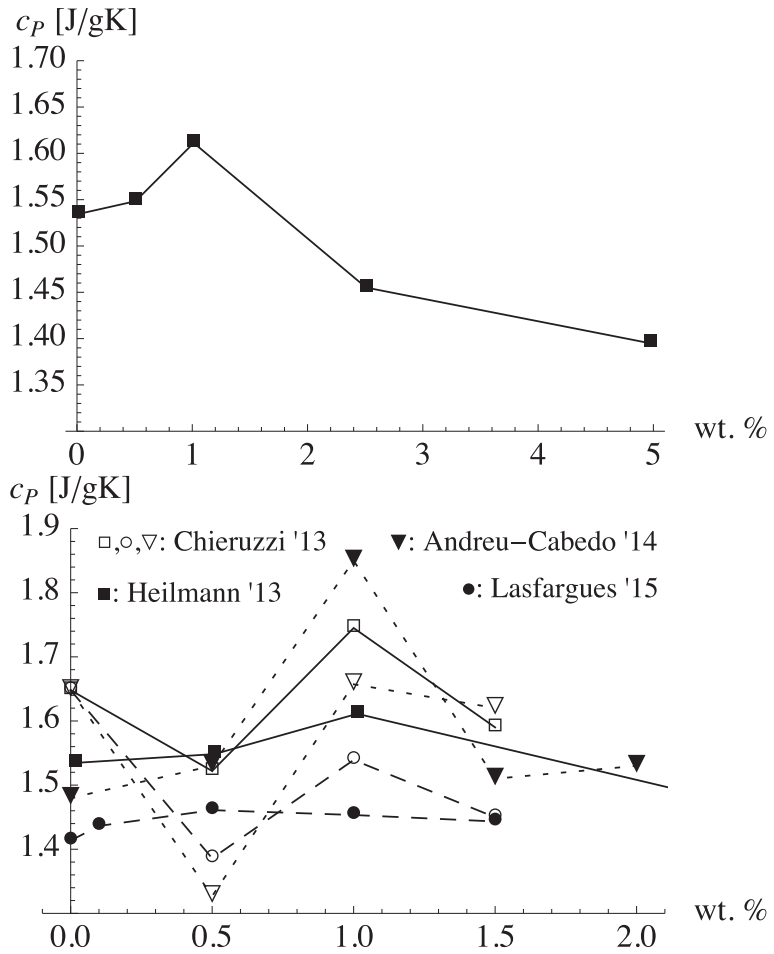

Fig. 3 Specific heat capacity of the nanofluid vs. particle mass fraction. *Top*: Specific heat capacity of the eutectic base mixture $NaNO_3/KNO_3$ (60:40) to which Al_2O_3 nanoparticles were added [33]. The temperature is 300 °C. *Bottom*: Specific heat capacity of the eutectic base mixture $NaNO_3/KNO_3$ (60:40). The *solid squares* again are Heilmann's data [33]. *Open squares* connected via a *solid line* are data obtained by Chieruzzi et al. [30] for the same system. The *circles* (*triangles*) are data obtained for the eutectic base mixture $NaNO_3/KNO_3$ (60:40) to which TiO_2 (SiO_2) nanoparticles were added. Open symbols are data by Chieruzzi et al. [30]. *Solid circles* indicate TiO_2 data by Lasfargues et al. [32]. *Solid triangles* indicate SiO_2 data by Andreu-Cabedo et al. [34]

We can refine this model and combine Eq. 5 with Eqs. 11 and 12 into a single expression. The underlying idea is depicted in Fig. 5. The sketch on the right shows a lattice model description of the nanofluid. Cells containing a box with a particle at their center are occupied by a nanoparticle including its interface layer. Cells may be occupied multiple times. Depicted is a single double occupied cell. Empty cells contain bulk base fluid, i.e., base fluid not affected by the presence of nanoparticles. Notice that in this model, there is no partial overlap. Interfacial layers overlap completely or not at all.

Assuming that the nanoparticles are uncorrelated, we may calculate the average volume base fluid, which is not affected by the presence of nanoparticles. Referring to the sketch, this is the average number of empty cells, n_e, on a cubic lattice possessing n_o cells into which n nanoparticles are placed randomly, i.e.,

$$n_e = n_o \exp[-n/n_o] \ . \tag{13}$$

Here, we also assume that n_o and n are large. Assuming that the liquid density inside the interface layer is the same (or nearly the same) as outside, we use the average liquid density $\bar{\rho} = \rho_{\rm np} x_{\rm np} + \rho_{\rm liq}(1 - x_{\rm np})$ to rewrite Eq. 13 into

$$x'_{\rm liq} = \frac{\rho_{\rm liq}}{\bar{\rho}} Y \tag{14}$$

with

$$Y = \exp\left[x_{\rm np} \left(x_{\rm np} + \frac{\rho_{\rm liq}}{\rho_{\rm np}} \left(1 - x_{\rm np}\right) \left(1 + \frac{\Delta}{R}\right)^3 \right) \right] . \tag{15}$$

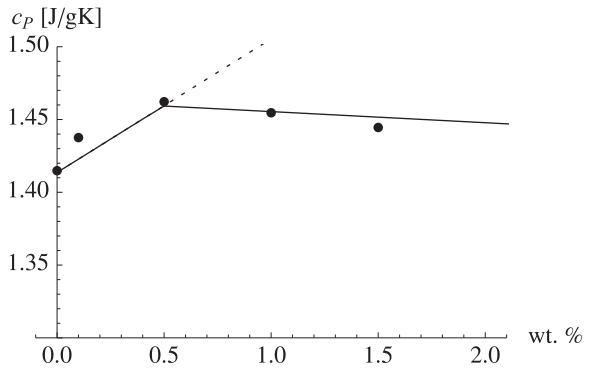

Fig. 4 Interacting mesolayer model compared to the experiment. Equation 5 in conjunction with Eqs. 11 and 12, (*solid line*) in comparison to the data of Lasfargues et al. [32] from Fig. 3 (*bottom panel*). The *dotted line* is the continuation of Eq. 5 beyond $x'_{\rm np}$

The quantity $x'_{\rm liq}$ is the mass fraction of bulk liquid, i.e., base liquid unaffected by the presence of nanoparticles. The specific heat capacity in this model is

$$c_P = \left[\kappa(1-x_{\rm np}) + (1-\kappa)x'_{\rm liq}\right] c_{p,{\rm liq}} + x_{\rm np} c_{P,{\rm np}} \,. \quad (16)$$

A comparison of this formula to experimental data is shown in Fig. 6. The expression works quite well in the case of the Lasfargues et al.'s data, whereas Heilmann's data are in mere qualitative agreement.

Improved agreement is achieved upon introducing a concentration independent κ. When the interfacial layers of two nanoparticles overlap, κ may be different in the overlap region in comparison to the part of the interface layer which is not overlapping. The dashed curves in Fig. 6 are obtained with a variable κ, which is given by

$$\kappa = \kappa_{\rm max} Y - \kappa_{\rm min}(1-Y) \,. \quad (17)$$

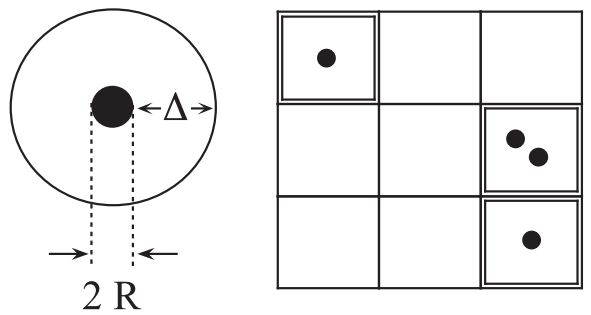

Fig. 5 Cell model. *Left*: A nanoparticle of radius R surrounded by its interface layer of thickness Δ. *Right*: Cubic lattice model of a nanofluid. Cells containing a box with a particle at their center are occupied by a nanoparticle including its interface layer. Cells may by occupied multiple times. Depicted is a single double occupied cell. Empty cells contain bulk base fluid, i.e., base fluid not affected by the presence of nanoparticles

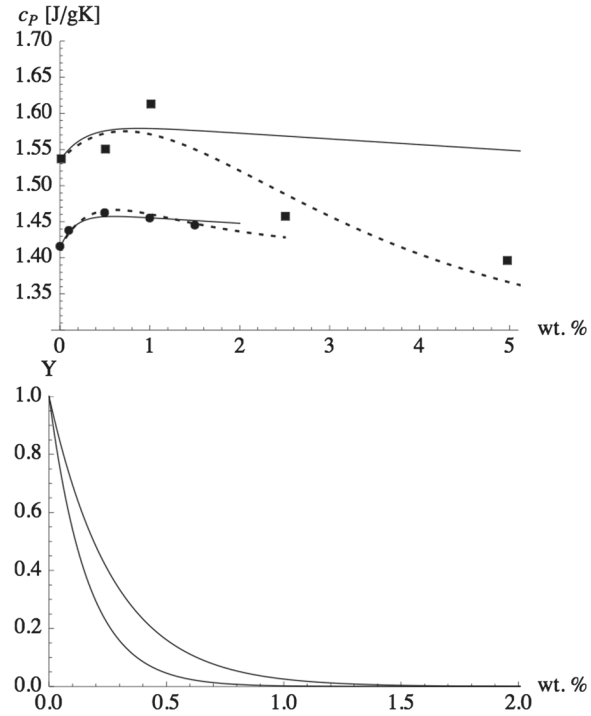

Fig. 6 Refined interacting mesolayer model compared to the experiment. *Top*: Equation 16 (*solid lines*) compared to the experiments of Lasfargues et al. [32] (*solid circles*) and Heilmann [33] (*solid squares*) from Fig. 3 (*bottom panel*). We use the experimental liquid densities of the respective source - even though the base salt is the same in both cases. Here, $\kappa = 1.035$ as in Fig. 4. $\Delta/R = 10$ in the case of the Lasfargues et al. data and $\Delta/R = 8$ in the case of the Heilmann data. In addition, we use $\rho_{\rm liquid} = 1.8$ g/cm^3, $\rho_{\rm TiO_2} = 3.9$ g/cm^3, $\rho_{\rm alumina} = 3.6$ g/cm^3, and $c_{P,{\rm np}}$ between 0.7 and 0.8 J/(gK). *Dashed lines*: Variable κ as explained in the text. Bottom: Y vs. weight percent corresponding to the two *solid lines* above. The *lower (upper) curve* corresponds to the fit of the Lasfargues (Heilmann) data

Notice that $\kappa = \kappa_{\rm max}$ when $Y = 1$, which means that little or no overlap between shells occurs on average. $\kappa = \kappa_{\rm min}$ when $Y = 0$. This means that the overlap is at a maximum. We use $\kappa_{\rm max} = 1.2(1.14)$, $\kappa_{\rm min} = 0.87(1.02)$, and $\Delta/R = 3.5(5.5)$ for the Heilmann (Lasfargues et al.) data. The theory now is in better agreement with both data sets. Notice that κ is reduced with increasing overlap.

But why should κ be reduced (below one) with increasing overlap? After all, our phenomenological model matches the experiments showing enhanced heat capacity only if $\kappa_{\rm max}$ is larger than one. The presence of a nanoparticle may apparently enhance the specific heat capacity in a surrounding liquid shell of width Δ by a factor $\kappa_{\rm max} > 1$. So why should the presence of a second nanaoparticle in the proximity of the first have the opposite effect? The interpretation is that increasing overlap means that nanoparticles may be getting close. This imposes significant positional ordering on the liquid molecules, which

may form a "solid-like" layer structure between the two "walls." This type of surface-induced ordering can for instance be measured using the surface force apparatus (e.g., [44]). Experiments show that $c_{P,\mathrm{solid}}$ of the base salt in its solid state is significantly lower than the corresponding $c_{P,\mathrm{liq}}$. An example is [26], where the authors provide both $c_{P,\mathrm{solid}}$ and $c_{P,\mathrm{liq}}$. Outside the immediate transition region, both specific heat capacities are well described by a linear dependence on temperature. If we linearly extrapolate $c_{P,\mathrm{solid}}$ into the temperature regime where $c_{P,\mathrm{liq}}$ is measured, then $c_{P,\mathrm{solid}}$ is up to 10 % less than $c_{P,\mathrm{liq}}$. Thus, if the c_p of the base liquid in this overlap area between nanoparticles becomes more like $c_{P,\mathrm{solid}}$, we should expect κ to decrease - even below one. Due to the complexity of the systems, we believe that this point should be studied using molecular simulation techniques rather than analytical approaches. The foremost question however remains - why is $\kappa_{\max}$ larger than one in the first place? We shall return to this question below.

When we discussed Fig. 1 (bottom panel) in the context of Eq. 5, we did reach the conclusion that $\kappa < 1$ was necessary to explain the data. In hindsight, we can now say that the decrease of c_P in the bottom panel of Fig. 1 as ϕ is increased is observed because the data, in the range $0.02 < x_{\mathrm{np}} < 0.1$, lie beyond the maximum of c_P for this nanofluid. This point is shown more clearly in Fig. 7. The figure combines the Heilmann data from Fig. 6 with the data from the bottom panel of Fig. 1. One of the dashed lines is again the upper dashed line from Fig. 6, i.e., the result of our recent theory with a variable κ parameter. In order to capture the particle size effect discussed in the context of Fig. 1 (bottom panel), a second curve with a slightly increased $\kappa_{\min}$ is needed. Notice the closeness of these values for $\kappa_{\min}$ to the κ values already conjectured during the previous discussion of the bottom panel of Fig. 1.

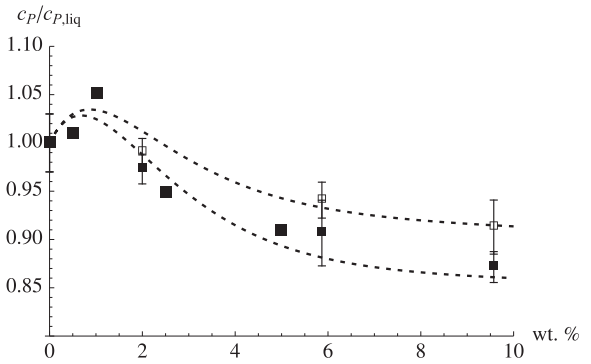

Fig. 7 Refined interacting mesolayer model with variable κ compared to the experiment. $c_P/c_{P,\mathrm{liq}}$ vs. weight percent nanoparticle. Comparison of the interacting mesolayer model with variable κ to experimental data. The larger *solid squares* are the Heilmann data (taken at 300 °C) from the previous figure. The smaller symbols including *error bars* are the data points shown in the *bottom panel* of Fig. 1 (based on averages in the temperature range from 290 to 335 °C). The lower of the two *dashed lines* agrees with the dashed line in the previous figure. The upper one, for the larger particles, is obtained by increasing $\kappa_{\min}$ from 0.87 to 0.93

We note that we did not alter the ratio Δ/R according to the two very different mean particle sizes used by Lu and Huang [25]. The ratio Δ/R determines the position of the c_P maximum in terms of nanoparticle concentration. We do not think that Δ and R are independent. The effect of nanoparticles on viscosity or, in the case of elastomers, the effect of nanoparticles on the elastic modulus is derived from hydrodynamic [45–47] or elastic equations [48]. The only length scale in these theories is the particle radius, R. The effect of the presence of a particle in the surrounding medium at a distance r from the particle center decays algebraically in terms of certain powers of R/r. We consider it very likely that the effect of the particles on c_P will follow from an analogous mathematical description. This means that Δ has no precise meaning. It should rather be thought of as some r at which R/r has decayed below a certain value. In this sense, we view Δ/R as one single parameter - independent of the actual particle radius.

However, we still need to tackle the question what possible mechanism leads to $\kappa_{\max} > 1$. Before addressing this point, we mention two observations, based on experimental evidence, which may provide helpful hints. First, it is worth noting that experimental studies find that the qualitative effect of nanoparticles on c_P appears to be the same in the solid and in the liquid state of the respective nanofluids (e.g., [21, 25–27, 35]). The solid state being of course not so much of technical importance. In the aforementioned studies, the solid state c_P rises close to linearly with increasing temperature in a rather wide range of temperatures. In most of these studies (exceptions are [26], where c_P is close to constant in the studied temperature range, and [35], where the authors find a decrease of c_P with rising temperature), this holds true also in the liquid state. These similarities between solid and liquid phase are interesting, because the solid state theory of specific heat capacity is much better developed than its counterpart for liquids. Secondly, we note that base salt mixtures like $NaNO_3/KNO_3$ (60:40) or the Li_2CO_3/K_2CO_3 eutectic (as well as water) possess a c_P, which is rather close to c_V calculated using the Dulong-Petit law.

One recent approach to the heat capacity in liquids, which explicitly exploits similarities between liquids and solids, is the phonon theory by Bolmatov et al. [49]. Bolmatov et al. show that their theory yields the isochoric heat capacity, C_V, vs. T for a great number of fluids in quite good quantitative agreement with experimental measurements. The key idea, based on an old proposition of Frenkel, is that a liquid becomes solid-like at frequencies larger than $\tau^{-1} \sim \eta^{-1}$, when it may support shear

waves. Here, τ is a certain relaxation time and η is the liquid's viscosity. The authors derive an expression for the internal energy of the liquid consisting of contributions due to longitudinal phonons as well as transverse (shear) phonons beyond τ^{-1} and a diffusion contribution below τ^{-1}. We emphasize this theory also because of one particular aspect. Since Einstein [45, 46], it is well known how the addition of dispersed particles to a liquid increases its viscosity, i.e., $\eta = \eta^*(1 + 2.5\phi)$ for $\phi \ll 1$ (cf. [3]). Here, η^* is the viscosity of the pure liquid and ϕ is the volume fraction of the added particles. In the present case, this means that τ^{-1} should decrease, i.e., the nanoliquid is able to support more shear modes at a particular temperature in comparison to the base fluid. This in turn increases C_V, and thus addition of nanoparticles, at first glance, leads to an increase of the isochoric heat capacity. However, the full relation between τ^{-1} and η^{-1} in [49] is $\tau^{-1} = G_\infty/\eta$, where G_∞ is the infinite-frequency shear modulus. Whether or not G_∞ possesses the same dependence on the concentration of added particles as η (cf. [48]) is a subtle question. If it does, then there is no effect of the nanoparticles on τ^{-1}. In the case of filled rubbers, which have much in common with liquids, it is well known that the glass transition is indeed not shifted by addition of nanoparticles (even at large amounts), i.e., the attendant relaxation times are not dependent on filler.

Even if the approach of Bolmatov et al. does not provide an immediate explanation of the enhanced c_P in nanofluids, we stick with the phonon idea and peruse it from another angle. The following is a simple example, illustrating how a small perturbation on the structure of the liquid, within the phonon picture of Bolmatov et al., may yield an increase of the heat capacity. Consider a one-dimensional perturbed, i.e., non-linear, oscillator, possessing the Hamiltonian

$$\mathcal{H} = \hbar\omega\left(-\frac{1}{2}\partial_q^2 + \frac{1}{2}q^2 - \lambda q^4\right). \tag{18}$$

Here, λ is a small parameter. First-order perturbation theory yields the energy eigenvalues $E_n = \hbar\omega(n + 1/2 + (3/2)\lambda(n^2 + n + 1/2))$. Notice that a q^3 perturbation does not contribute in the first order, and this is why a q^4 perturbation is considered here instead. We obtain C_V via $C_V = \partial\langle E\rangle/\partial T|_V$ and $\langle E\rangle = \partial_{(-\beta)} \ln\sum_{n=0}^{\infty} \exp[-\beta E_n]$, where $\beta = (k_B T)^{-1}$. Assuming that $\beta\hbar\omega\lambda \ll 1$, we use the expansion $\exp[-\beta E_n] \approx (1 - \hbar\omega(3/2)\beta\lambda(n^2 + n + 1/2))\exp[-\beta\hbar\omega(n + 1/2)]$, which yields

$$C_V/k_B \approx 1 + 6\lambda t - 1/\left(12t^2\right) \tag{19}$$

in leading order of (small) λ and (large) $t = k_B T/(\hbar\omega)$. Had we included a term χq^3 in $\mathcal{H}$, then its leading order contribution to C_V would have been $15\chi^2 t$. Figure 8 compares Eq. 19 to the exact C_V of the harmonic oscillator

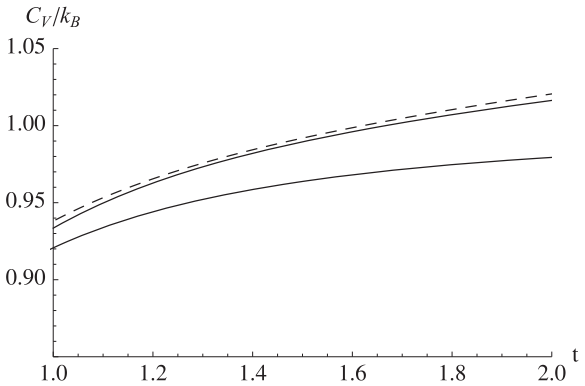

Fig. 8 Heat capacity of a one-dimensional perturbed oscillator. C_V/k_B vs. reduced temperature $t = k_B T/(\hbar\omega)$. The *lower (upper) solid line* is the result for the harmonic (perturbed) oscillator, i.e., $\lambda = 0(0.01)$. The *dashed line* is the numerical solution of the perturbed oscillator's heat capacity

($\lambda = 0$) as well as to the numerical solution of the perturbed oscillator according to Eq. 19. The figure illustrates that even a small perturbation (here, $\lambda = 0.01$) yields a significant increase of C_V at high temperatures. Note that when λ is positive, the perturbation increases the width of the oscillator potential, which reduces the spacing between eigenvalues and thus increases C_V. What we propose is in essence that the nanoparticles induce a long-range perturbation into the surrounding liquid (or solid in the case of the solid phase), which gives rise to enhanced anharmonicity.

Notice that anharmonic molecular interactions are the source of thermal expansion. Both heat capacity and thermal expansion are closely related - at least in the case of solids (e.g., § 67 in [50]; To the best of the author's knowledge, this particular relation has not been explored thus far in experiments on nanofluids in the present context. Thermal expansion of water-based nanofluids has been obtained in several studies primarily aimed at quantities other than heat capacity (e.g., [51]). But in these water-based systems, excess effects due to the presence of nanoparticles are difficult to discern.) Because the expression Bolmatov et al. derive for C_V, based on their phonon theory, also contains the thermal expansion coefficient (in fact, their C_V increases with increasing thermal expansion), the calculation or modeling of the latter may offer a theoretical approach to c_P. At least from the perspective of molecular computer simulation, thermal expansion appears to be the simpler quantity.

We remark in closing that recently, Tiznobaik, Shin, and Banerjee [28, 29] have carried out an interesting experiment, which shows that addition of NaOH in minuscule amounts prevents the formation of structure and eliminates the previously observed c_P enhancement. In the

present picture, we would interpret the effect of NaOH as one that relaxes anharmonicity effects.

Conclusions

Specific heat enhancements of the type observed thus far requires one or both of the following to be true: (i) Every particle is surrounded by a nanolayer with a c_P exceeding the bulk fluid's c_P by a large factor. This is necessary to explain the large increases observed in some experiments in which c_P is enhanced through addition of minute amounts of nanoparticle to the base fluid. (ii) The effect of the particles on the base fluid has a long range (100 nm or more), which only requires a moderate change of c_P in the attendant mesolayer. The new phenomenological theory, i.e., the interacting mesolayer model, developed on the assumption of (ii) can explain the occurrence of the c_P vs x_{np} maximum. It contains three parameters: (1) Δ/R, i.e., the width of the mesolayer in units of R, the particle radius; (2) $\kappa_{\max}$, the ratio of the average specific heat capacity inside the mesolayer at vanishing overlap to the specific heat capacity of the base fluid at the same temperature; (3) $\kappa_{\min}$, the ratio of the average specific heat capacity inside the mesolayer at maximum overlap to the specific heat capacity of the base fluid at the same temperature. Thus far, no microscopic theory exists, from which these parameters can be computed. Nevertheless, we have proposed a physical picture according to which $\kappa_{\max} > 1$ is possible, based on induced enhanced anharmonicity of the molecular interactions, as well as a mechanism for the reduction of κ to $\kappa_{\min}$, via 'solidification' of the base liquid due to confinement.

Abbreviations

BET: Brunauer-Emmett-Teller; CTAB: dodecyl-trimethyl-ammonium; CNT: carbon nanotubes; SDS: sodium-dodecyl-sulfate; TEM: transmission electron micrograph.

Competing interests

The author declares that he has no competing interests.

Acknowledgements

This work was supported through DFG-grant HE 1545/18-1.

Received: 15 September 2015 Accepted: 1 December 2015
Published online: 13 February 2016

References

1. Thirugnanasambandam M, Iniyan S, Goic R (2010) A review of solar thermal technologies. Renew Sustain Energy Rev 14:312–322
2. Shahrul IM, Mahbubul IM, Khaleduzzaman SS, Saidur R, Sabri MFM (2014) A comparative review on the specific heat of nanofluids for energy perspective. Renew Sustain Energy Rev 38:88–98
3. Ilyas SU, Pendyala R, Shuib A, Marneni N (2014) A review on the viscous and thermal transport properties of nanofluids. Adv Mater Res 917:18–27
4. Choi SUS (1995) Enhancing thermal conductivity of fluids with nanoparticles. In: Developments and Applications of Non-Newtonian Flows vol. ASME Publications FED-Vol. 231/MD-Vol. 66. The American Society of Mechanical Engineers, New York. pp 99–105
5. Xuan Y, Li Q (2000) Heat transfer enhancement of nanofluids. Int Commun Heat Mass 21:58–64
6. Patel HE, Das SK, Sundararajan T, Nair AS, George B, Pradeep T (2003) Thermal conductivities of naked and monolayer protected metal nanoparticle based nanofluids: manifestation of anomalous enhancement and chemical effects. Appl Phys Lett 83:2931–2933
7. Liu MS, Ching-Cheng Lin M, Huang IT, Wang CC (2005) Enhancement of thermal conductivity with carbon nanotube for nanofluids. Int Commun Heat Mass 32:1202–1210
8. Liu MS, Lin MC-C, Tsai CY, Wang CC (2006) Enhancement of thermal conductivity with Cu for nanofluids using chemical reduction method. Int J Heat Mass Transf 49:3028–3033
9. Namburu PK, Kulkarni DP, Dandekar A, Das DK (2007) Experimental investigation of viscosity and specific heat of silicon dioxide nanofluids. Micro Nano Lett 2:67–71
10. Kulkarni DP, Vajjha RS, Das DK, Oliva D (2008) Application of aluminum oxide nanofluids in diesel electric generator as jacket water coolant. Appl Therm Eng 28:1774–1781
11. Vajjha RS, Das DK (2009) Specific heat measurement of three nanofluids and development of new correlations. J Heat Transf 131:071601
12. Zhou SQ, Ni R (2008) Measurement of the specific heat capacity of water-based Al_2O_3 nanofluid. Appl Phys Lett 92:093123
13. O'Hanley H, Buongiorno J, McKrell T, Hu LW (2012) Measurement and model validation of nanofluid specific heat capacity with differential scanning calorimetry. Adv Mechanical Eng 4:181079
14. Sekhar YR, Sharma KV (2015) Study of viscosity and specific heat capacity characteristics of water-based Al_2O_3 nanofluids at low particle concentrations. J Exp Nanosci 10:86–102
15. Nelson IC, Banerjee D, Ponnappan R (2009) Flow loop experiments using polyalphaolefin nanofluids. J Thermophys Heat Transfer 23:752–761
16. Shin D, Jo B, Kwak H, Banerjee D (2010) Investigation of high temperature nanofluids for solar thermal power conversion and storage applications. In: 14th International Heat Transfer Conference, Washington, DC. ASME, New York. pp 583–591
17. Jo B, Banerjee D (2014) Enhanced specific heat capacity of molten salt-based nanomaterials: effects of nanoparticle dispersion and solvent material. Acta Materialia 75:80–91
18. Jo B, Banerjee D (2015) Enhanced specific heat capacity of molten salt-based carbon nanotubes nanomaterials. J Heat Transfer 137:091013
19. Zhou LP, Wang BX, Peng XF, Du XZ, Yang YP (2009) On the specific heat capacity of CuO nanofluid. Adv Mechanical Eng 2:172085
20. Shin D, Banerjee D (2011) Enhancement of specific heat capacity of high-temperature silica-nanofluids synthesized in alkali chloride salt eutectics for solar thermal-energy storage applications. Intl J Heat Mass Transfer 54:1064–1070
21. Shin D, Banerjee D (2010) Effects of silica nanoparticles on enhancing the specific heat capacity of carbonate salt eutectic (work in progress). Int J Struct Changes Solids - Mech Appl 2:25–31
22. Shin D, Banerjee D (2011) Enhanced specific heat of silica nanofluid. J Heat Transfer 133:024501
23. Shin D, Banerjee D (2013) Enhanced specific heat capacity of nanomaterials synthesized by dispersing silica nanoparticles in eutectic mixtures. J Heat Transfer 135:032801
24. Shin D, Banerjee D (2014) Specific heat of nanofluids synthesized by dispersing alumina nanoparticles in alkali salt eutectic. Int J Heat Mass Transfer 74:201–214
25. Lu MC, Huang CH (2013) Specific heat capacity of molten salt-based alumina nanofluid. Nanoscale Res Lett 8:292–299
26. Dudda B, Shin D (2013) Effect of nanoparticle dispersion on specific heat capacity of binary nitrate salt eutectic for concentrated solar power applications. Int J Thermal Sci 69:37–42
27. Tiznobaik H, Shin D (2013) Enhanced specific heat capacity of high-temperature molten salt-based nanofluids. Int J Heat Mass Transfer 57:542–548
28. Tiznobaik H, Shin D (2013) Experimental validation of enhanced heat capacity of ionic liquid-based nanomaterial. Appl Phys Lett 102:173906
29. Shin D, Tiznobaik H, Banerjee D (2014) Specific heat mechanism of molten salt nanofluids. Appl Phys Lett 104:121914
30. Chieruzzi M, Cerritelli GF, Miliozzi A, Kenny JM (2013) Effect of nanoparticles on heat capacity of nanofluids based on molten salts as PCM for thermal energy storage. Nanoscale Res Lett 8:448–457
31. Lasfargues M (2014) Nitrate based high temperature nano-heat-transfer-fluids: formulation & characterisation. PhD thesis. University of Leeds

32. Lasfargues M, Geng Q, Cao H, Ding Y (2015) Mechanical dispersion of nanoparticles and its effect on the specific heat capacity of impure binary nitrate salt mixtures. Nanomaterials 5:1136–1146
33. Heilmann P (2013) Evaluation, neuentwicklung und optimierung des eigenschaftsprofils von salzschmelzen für die verwendung als wärmeträgerfluide. PhD thesis. Bergische Universität, Wuppertal
34. Andreu-Cabedo P, Mondragon R, Hernandez L, Martinez-Cuenca R, Cabedo L, Julia JE (2014) Increment of specific heat capacity of solar salt with SiO_2 nanoparticles. Nanoscale Res Lett 9:582–592
35. Chieruzzi M, Miliozzi A, Crescenzi T, Torre L, Kenny JM (2015) A new phase change material based on potassium nitrate with silica and alumina nanoparticles for thermal energy storage. Nanoscale Res Lett 10:273–282
36. Ho MX, Pan C (2014) Optimal concentration of alumina nanoparticles in molten Hitec salt to maximize its specific heat capacity. Int J Heat Mass Transfer 70:174–184
37. Paul TC (2014) Investigation of thermal performance of nanoparticle enhanced ionic liquids (NEILs) for solar collector applications. PhD thesis. University of South Carolina
38. Wang BX, Zhou LP, Peng XF (2006) Surface and size effects on the specific heat capacity of nanoparticles. Int J Thermophysics 27:139–151
39. Saeedian M, Mahjour-Shafiei M, Shojaee E, Mohammadizadeh MR (2012) Specific heat capacity of TiO2 nanoparticles. J Comput Theor Nanosci 9:616–620
40. Röthemeyer F, Sommer F (2013) Kautschuktechnologie. Hanser Verlag, München
41. Evans DF, Wennerström H (1994) The colloidal domain. VCH, New York
42. Stanley HE (1971) Introduction to phase transitions and critical phenomena. Oxford University Press, New York
43. Oyen E, Hentschke R (2002) Molecular dynamics simulation of aqueous sodium chloride solution at the NaCl(001) interface with a polarizable water model. Langmuir 18:547–556
44. Israelachvili J (1991) Intermolecular and surface forces. Academic Press, London
45. Einstein A (1906) Eine neue bestimmung der moleküldimension. Ann d Physik 19:289–306
46. Einstein A (1911) Eine neue bestimmung der moleküldimension (korrektur). Ann d Physik 34:591–592
47. Felderhof BU (1990) Hydrodynamic of suspensions. In: van Beijren H (ed). Fundamental Problems in Statistical Mechanics VII. North-Holland, Amsterdam
48. Smallwood HM (1944) Limiting law of the reinforcement of rubber. J Appl Phys 15:758–766
49. Bolmatov D, Brazhkin VV, Trachenlo K (2012) The phonon theory of liquid thermodynamics. Sci Rep 2:421–426
50. Landau LD, Lifshitz EM (1980) Statistical physics (Vol. 5). Elsevier, Oxford
51. Khanafer K, Vafai K (2011) A critical synthesis of thermophysical characteristics of nanofluids. Int J Heat Mass Transfer 54:4410–4428